Fused Porphyrin–Single-Walled Carbon Nanotube Hybrids: Efficient Formation and Photophysical Characterization

Qiwen Zhong, Vyacheslav V. Diev, Sean T. Roberts, Priscilla D. Antunez, Richard L. Brutchey, Stephen E. Bradforth, and Mark E. Thompson*

Department of Chemistry, University of Southern California, Los Angeles, California 90089, United States

ABSTRACT A systematic study of the interaction between π-extended porphyrins and single-walled carbon nanotubes (SWNTs) is reported here. Zinc porphyrins with 1-pyrenyl groups in the 5,15-*meso* positions, 1, as well as compounds where one or both of the pyrene groups have been fused at the *meso* and β positions of the porphyrin core, 2 and 3, respectively, have been examined. The strongest binding to SWNTs is observed for porphyrin 3, leading to debundling of the nanotubes and formation of stable suspensions of 3–SWNT hybrids in a range of common organic solvents. Absorption spectra of 3–SWNT suspensions are broad and continuous (λ = 400–1400 nm), and the Q-band of 3 displays a significant bathochromic shift of 33 nm. The surface coverage of the SWNTs in the nanohybrids was estimated by spectroscopic and analytical methods and found to reach 64% for (7,6) nanotubes. The size and shape of π-conjugated porphyrins were found to be important factors in determining the strength of the π–π interactions, as the linear *anti*-3 isomer displays more than 90% binding selectivity compared to the bent *syn*-3 isomer. Steady-state photoluminescence measurements show quenching of porphyrin emission from the nanohybrids. Femtosecond transient absorption spectroscopy reveals that this quenching results from ultrafast electron transfer from the photoexcited porphyrin to the SWNT ($1/k_{CT}$ = 260 fs) followed by rapid charge recombination on a picosecond time scale. Overall, our data demonstrate that direct π–π interaction between fused porphyrins and SWNTs leads to electronically coupled stable nanohybrids.

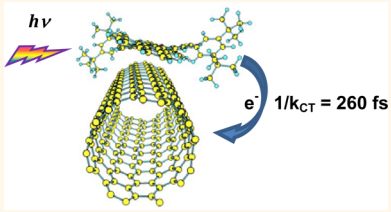

KEYWORDS: π-extended porphyrins · noncovalent π–π interaction · single-walled carbon nanotubes · nanohybrids · isomer selectivity · femtosecond transient absorption · ultrafast electron transfer

Single-walled carbon nanotubes (SWNTs) have unique optical,[1–4] mechanical,[5–7] and electronic[8,9] properties that have been utilized in a wide range of applications in fields such as biology, molecular electronics, and solar energy conversion.[10–15] However, the polydispersity and insolubility of SWNTs in common organic solvents and water hamper the extension of SWNTs to further applications.[16] Among efforts to increase the processability of SWNTs, the noncovalent binding of small molecules or polymers to SWNT surfaces is a powerful strategy to introduce chemical functionalities to SWNTs without significantly affecting the structure and electronic properties of the nanotubes.[17,18] In this context, polycyclic aromatic molecules and conjugated polymers have been used to modify and disperse SWNTs by forming π–π interactions with nanotube sidewalls.[19,20] The attachment of functional units to SWNTs through the formation of solubilizing π–π interactions offers great opportunity to develop SWNT-based hybrids for various applications. In particular, SWNT-based photosensitizing donor–acceptor multichromophore nanohybrids[21,22] are promising materials for photovoltaic applications due to their light-harvesting characteristics and the excellent charge transport properties of SWNTs.[23,24]

Chromophores have been tethered to polycyclic aromatic compounds, such as pyrene, which noncovalently bind to SWNT surfaces through π–π interactions,[25,26] but the spatial distance between the chromophores and the SWNT surface can hinder desirable electronic coupling in such photosensitized donor–acceptor hybrids. Heterocyclic polyaromatic molecules such as

* Address correspondence to met@usc.edu.

Received for review January 23, 2013 and accepted March 10, 2013.

Published online March 10, 2013
10.1021/nn400362e

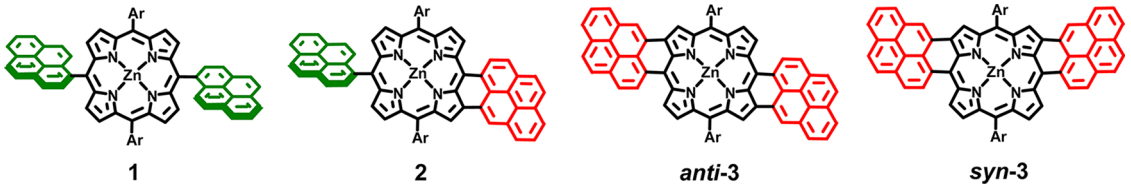

Figure 1. Structures of nonfused bis-pyrenyl porphyrin 1, monofused pyrenyl porphyrin 2, and doubly fused pyrenyl porphyrin 3 including the isomers *anti*-3 and *syn*-3. Ar indicates 3,5-di-*tert*-butylphenyl groups.

porphyrins[27,28] can bind more directly to SWNTs through the π-system of the chromophores, resulting in porphyrin−SWNT hybrids with the potential for improved electronic coupling between the SWNT and bound chromophore. However, these hybrids can be easily dissociated, indicating a weak affinity for the SWNT surface. Due to the larger size of their π-system, triply connected porphyrin tapes[29,30] and polymers[31] were found to display a larger binding affinity for SWNTs compared to porphyrin monomers. However, these conjugated porphyrins not only are difficult to synthesize but also display limited solubility and processability. Moreover, making a stable suspension using triply connected porphyrins is possible only in trifluoroacetic acid-containing solvents or by adding multiple bulky alkyl groups to the porphyrin tape.[30] The further rational design of photoactive SWNT donor−acceptor hybrids requires a fundamental understanding of the noncovalent chemistry, the nature of $\pi-\pi$ interactions between light-harvesting molecules and SWNTs, and its effect on photosensitized energy and electron transfer processes.

Large π-extended porphyrins obtained by the fusion of porphyrin to *meso*-connected polycyclic aromatic rings have attracted significant attention recently.[32−39] Among them, porphyrins fused at *meso*, β positions with unsubstituted polycyclic aromatic rings represent unique types of large π-systems that are not sterically blocked and thus available to form $\pi-\pi$ stacking interactions with SWNT surfaces.[38,39] At the same time these porphyrins have improved solubility in organic solvents due to out-of-plane distortions of the porphyrin core that prevent strong aggregation. Previously, we demonstrated that such porphyrins can exhibit $\pi-\pi$ interactions with each other and also with fullerenes, as evidenced by a significant bathochromic shift of the porphyrin Q-band transition in thin film absorption spectra.[38,39]

In this study, we have probed the concept of using the unhindered π-system of fused porphyrins, minimizing the spatial distance between the porphyrin chromophore and the SWNT surface, to enhance their affinity to bind to SWNT sidewalls and to facilitate electronic coupling. We chose nonfused bis-pyrenyl porphyrin **1**, monofused pyrenyl porphyrin **2**, and the doubly fused pyrenyl porphyrins *anti*-**3** and *syn*-**3**, shown in Figure 1, to systematically study how extending the size and shape of the π-systems of these pyrenyl-porphyrins modifies their interaction with SWNTs.

We demonstrate the first example of stable and easily processable nanohybrids formed by strong noncovalent interactions between SWNTs and π-extended porphyrins in nonpolar organic solvents. These porphyrin−SWNT hybrids show very promising light-harvesting properties, possessing absorption transitions that span from the visible to the NIR due to complementary absorption features of the porphyrin chromophore and SWNTs. The binding interaction between SWNTs and attached porphyrins not only displays selectivity toward specific porphyrin isomers but is also sufficiently strong to prevent dissociation of the porphyrin from the SWNT when strongly coordinating ligands are added, allowing further hierarchical modification by metal−ligand axial coordination without disturbing the stability of the hybrids. Femtosecond transient absorption experiments reveal the presence of ultrafast photoinduced electron transfer between porphyrin molecules and the SWNT to which they are bound, but also show rapid electron−hole recombination following electron transfer.

RESULTS AND DISCUSSION

The formation of noncovalent $\pi-\pi$ interactions between nanotube sidewalls and conjugated materials, including aromatic molecules and conjugated polymers, is a useful and simple approach to modify and disperse SWNTs. The solubilizing ability of different conjugated materials has been shown to depend on the size of the π-system of the noncovalent modifier. For example, pyrene groups adsorb onto SWNTs and impart solubility to the nanotubes, whereas phenanthrene binding groups show only limited solubilizing ability and naphthalene binding groups have no solubilizing affect.[40] In addition, the affinity of conjugated porphyrin oligomers to bind to SWNTs was demonstrated to increase sharply with the length of the porphyrin's π-system.[41]

To determine the affinity with which pyrenyl porphyrins **1**, **2**, and **3** bind to SWNTs, porphyrin−SWNT suspensions were prepared by sonicating SWNTs with porphyrin solutions. **1**, **2**, and **3** were prepared as previously described.[38,39] Compound **3** is obtained as a 1:1 mixture of *anti* and *syn* isomers. Sonication of SWNTs with solutions of **2** or **3** for approximately

one hour results in a homogeneous suspension of SWNTs, whereas insoluble SWNTs aggregates could still be observed when **1** was employed. Formation of a well-dispersed suspension was found to occur in a wide range of solvents, including dimethylformamide (DMF), chlorobenzene, CH_2Cl_2, THF, and toluene. The suspensions of SWNTs with **1**, **2**, and **3** were filtered through a 0.4 μm pore polytetrafluoroethylene (PTFE) membrane and washed repeatedly with the solvent used for sonication until the filtrate was colorless, indicating the removal of any excess/unbound porphyrin.[29,30] The prepared porphyrin–SWNT hybrids could be quantitatively resuspended after filtration and washing. The **1**–SWNT suspension began to precipitate upon standing for an hour in the absence of excess porphyrin, while **2**–SWNT did not show precipitation within 24 h of preparation but started aggregating after a week. In contrast, **3**–SWNT showed no sign of precipitation after a week of standing without the presence of excess porphyrin.

Absorption spectroscopy was used to characterize suspensions of these porphyrin–SWNT hybrids. Optical absorption spectra of the porphyrin–SWNT hybrids along with spectra of the individual components are shown in Figure 2. Compounds **1**, **2**, and **3** display Soret and Q-band absorptions characteristic of porphyrins below and above 550 nm, respectively, which red-shift and broaden as the π-system of the porphyrin is extended through consecutive pyrene fusion. The Soret and Q-band absorptions of **1** (λ_{max} = 429 and 560 nm, respectively) did not change upon suspending with SWNTs, while those of **2** (λ_{max} = 498 and 725 nm, respectively) broadened and red-shifted to 500 and 743 nm following the addition of SWNTs to solution, indicating interaction between **2** and the added SWNTs. The broad features attributed to SWNT absorption in the region of λ = 1000–1400 nm are unaltered by the presence of **2**, suggesting that many of the SWNTs present in solution do not directly interact with **2**, possibly due to the presence of large SWNT bundles. Absorption bands of **3** are observed at 510, 530, and 834 nm and show a similar broadening and red-shift to 512, 534, and 867 nm once SWNTs are added to the solution. In the region of λ = 1000–1400 nm, SWNTs show distinct absorption features that are narrower and better resolved with respect to the absorption of a pristine SWNT suspension, suggesting substantial if not complete dissociation of the SWNT bundles.

The dissociation of SWNT bundles by **3** into small bundles or individual SWNTs was further confirmed by transmission electron microscopy (TEM) characterization of the hybrids. Before modification by **3**, SWNTs are aggregated (Figure 3A), forming a dense network of bundles due to strong internanotube van der Waals attractions. In contrast, **3**–SWNT shows substantial unwinding of the aggregates into small bundles or individual tubes (Figure 3B), indicating that π–π

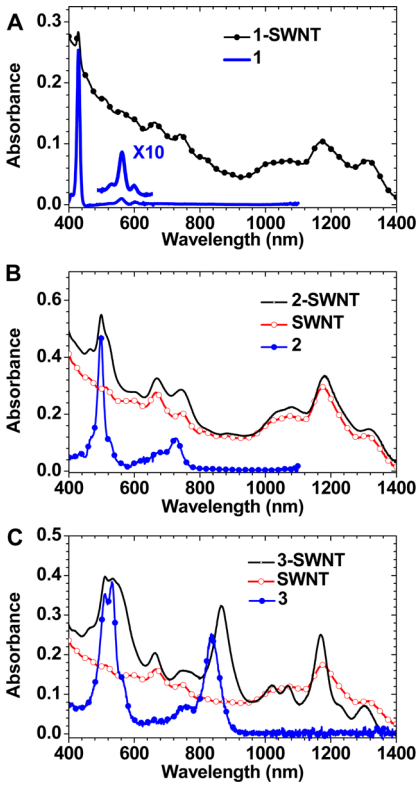

Figure 2. Absorption spectra of (A) nonfused bis-pyrenyl porphyrin 1 and 1–SWNT hybrids in DMF. Inset: Porphyrin Q-band at 560 nm. (B) Monofused porphyrin 2, CoMoCAT SWNTs, and 2–SWNT hybrids in DMF. (C) Doubly fused porphyrin 3, CoMoCAT SWNTs, and 3–SWNT hybrids in DMF.

interactions between **3** and the SWNT surface are strong enough to overcome internanotube van der Waals attraction and prevent SWNTs from rebundling after formation of the porphyrin–SWNT hybrids.

To further investigate the interaction between **3** and SWNTs, we varied the ratio between **3** and SWNTs in solution, and instead of filtering off unbound porphyrin after an hour of probe sonication, ultracentrifigation for 30 min at 42000*g* was used to remove large SWNT bundles. Absorption spectra of the supernatant solution after centrifugation are shown in Figure 4A. When an excessive amount of **3** was used (*i.e.*, 2:1 weight ratio), absorption spectra of the supernatant solution show both free porphyrin and **3**–SWNT hybrid features. As the amount of **3** was reduced (1:1), no absorption from free porphyrin was observed in the supernatant, suggesting an irreversible attachment of **3** to SWNTs. When the weight ratio between **3** to SWNT fell below 0.3, the supernatant became colorless and displayed no absorption from either **3** or SWNTs, suggesting the amount of **3** was not enough to break apart SWNT bundles, so that both **3** and SWNTs are quantitatively removed by ultracentrifigation from solution. Therefore a threshold porphyrin to SWNT ratio exists for efficient SWNT dispersion. When a mixture of **1**, **2**, and **3** is used, only the free porphyrin absorption of

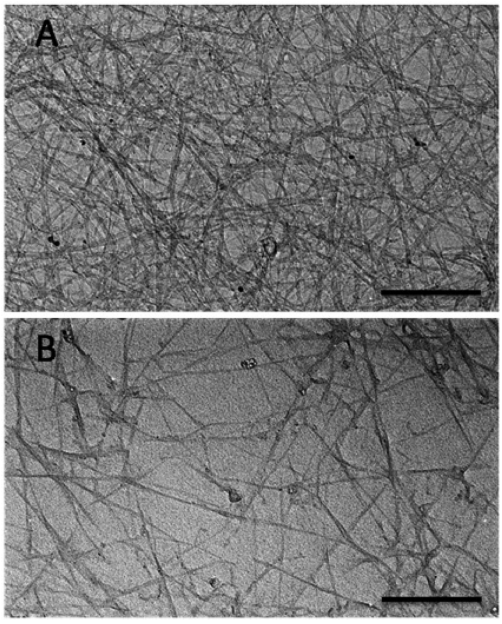

Figure 3. (A) TEM characterization of the SWNT sample before porphyrin 3 modification and (B) after modification. The black scale bar in both images indicates 200 nm.

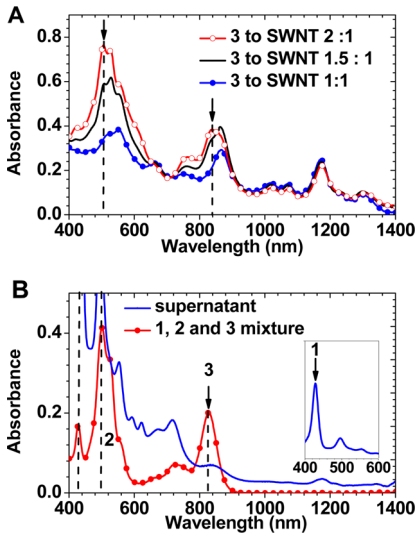

Figure 4. Absorption spectra of the supernatant. (A) Samples with different 3 to SWNT weight ratios. Black arrows indicate the disappearance of absorption features from free porphyrin 3. (B) Samples with a mixture of porphyrins 1, 2, and 3 (red: initial porphyrin mixture absorption; blue: supernatant after sonication with SWNTs and centrifugation). Inset: Supernatant absorption at 400–600 nm plotted on an expanded scale.

1 and **2** is observed in the supernatant, with **1** being enriched, while absorptions corresponding to either free SWNTs or **3** are not observed (Figure 4B), suggesting that **3** has the highest binding affinity for SWNTs, followed by **2** and lastly **1**. This study provides strong evidence that the degree of interaction between monoporphyrins and SWNTs can be increased through the extension of the π-system of monoporphyrins. Even though **1** is singly connected to two pyrenyl groups, a functional group well known to bind to SWNTs,[42] steric hindrance between porphyrin and pyrenyl rings in the structure of **1** prevents the binding of either pyrene moiety or porphyrin core to the sidewalls of the SWNTs. Upon pyrene fusion, steric hindrance was eliminated and the extended π-conjugation enhanced the binding interactions between either **2** or **3** and SWNTs.

Possible detachment of **3** from SWNTs was investigated by repeating the washing, filtering, and resuspension cycle of the **3**–SWNT hybrids. The relative absorbance of the porphyrin compared to that of SWNTs was unchanged after three cycles (Figure 5A), indicating no measurable detachment of **3** from SWNTs. Moreover, no detachment of **3** from SWNTs was observed following the addition of coordination additives, such as pyridine and dodecylamine, to **3**–SWNT suspensions. While the added amines did not lead to release of **3**, the porphyrin Q-band absorption of the nanohybrids displayed a red-shift (Figure 5B) due to the coordination of the additives to **3**. Similar red-shifted Q-band absorption was observed when the same additives were added to the porphyrin solution (see Supporting Information Figure S1). This coordination reaction allows for further modification of **3**–SWNT hybrids by metal–ligand axial coordination without disturbing the stability of the hybrids.

Modification Ratio Estimation. The fraction of the SWNT surface covered by **3** in **3**–SWNT hybrids was estimated by two methods, absorption spectroscopy and elemental analysis. In the first method, the amount of bound **3** in the nanohybrids was estimated by using the molar absorptivity of the Q-band for **3** in CH_2Cl_2 at 867 nm (1.1×10^5 M^{-1} cm^{-1}), assuming this value remains unchanged upon binding to SWNTs. The nanohybrids were prepared using a measured amount of SWNTs and an excess of **3**. After filtration of **3**–SWNT and repeated washing to eliminate excess **3**, the **3**–SWNT sample was suspended in a fixed volume of DMF and the absorption spectrum measured to estimate the amount of **3** in the **3**–SWNT sample. The measured modification ratio was 177 SWNT carbon atoms per molecule of **3**. To estimate the percentage of the SWNT surface covered by **3**, we consider the fact that we used a CoMoCAT SWNT mixture, which contains a majority (>50%) of (7,6) semiconducting SWNTs. (7,6) SWNTs have a diameter of 0.88 nm with 508 carbon atoms per unit cell. Given the measured modification ratio, we estimate that 2.9 molecules of **3** exist per unit cell of (7,6) SWNT.

The modification ratio was also evaluated by elemental analysis of the unbound **3** in the filtrate from the absorbance measurement. Unbound **3** was first demetalated, followed by EDTA titration to determine the Zn concentration. Given that each porphyrin molecule coordinates a single Zn atom, the titrated amount of Zn in the filtrate is complementary to that

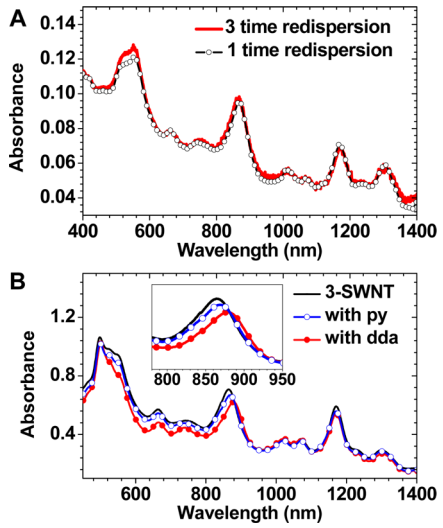

Figure 5. Absorption spectra of 3—SWNT hybrids (A) after one and three cycles of washing, filtering, and redispersing and (B) with pyridine (py) and dodecylamine (dda) as coordination ligands.

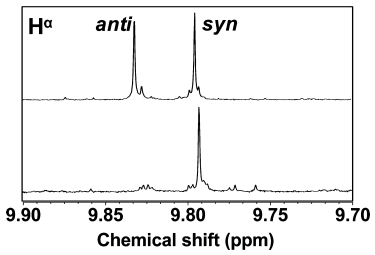

Figure 6. Top: NMR spectrum of 3 before modification with SWNTs. Bottom: NMR spectrum of the filtrate following the addition of SWNTs.

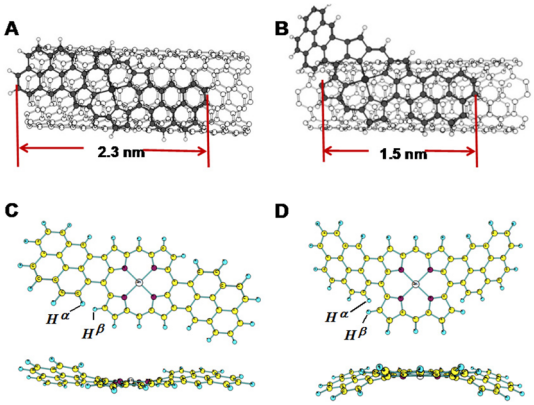

Figure 7. (A and B) Comparison of the π-system size and shape of *anti*-3 and *syn*-3 with that of the SWNT along the SWNT's long axis. (C and D) Optimized structures of model porphyrins *anti*-3 and *syn*-3 without the 3,5-di-*tert*-butylphenyl groups, calculated at the B3LYP/6-31G*/LANL2DZ level. Reprinted with permission from V. V. Diev, C. W. Schlenker, K. Hanson, Q. Zhong, J. D. Zimmerman, S. R. Forrest, and M. E. Thompson, *J. Org. Chem*. 2012, *77*, 143. Copyright 2012, American Chemical Society.

in the porphyrin—SWNT hybrids. The modification ratio determined by this method was 157 SWNT carbon atoms per molecule of **3**, which is nearly double the modification ratio of 280 carbon atoms to 1 molecule of previously reported pyrene derivatives.[43] On the basis of a (7,6) SWNT, the modification ratio was estimated to be 3.2 molecules of **3** per unit cell of (7,6) SWNT, reaching a 64% surface coverage of SWNT. The estimated modification ratios from both absorption spectroscopy and elemental analysis are in good agreement given that our modification ratio calculated from the molar absorptivity of **3** does not account for the broadening and red-shifting of the porphyrin Q-band upon binding to SWNTs. If the oscillator strength of the porphyrin Q-band is preserved upon SWNT binding, our methodology will lead to an underestimation of the amount of porphyrin bound to the SWNT surface.

The molecular morphology of the pyrene-fused porphyrins was also investigated. As aforementioned, the as-synthesized **3** was a 1:1 mixture of *anti* and *syn* isomers. In both isomers, the length of the cavity between the two di-*tert*-butylphenyl groups is 0.89 nm, matching well the diameter of (7,6) SWNTs. The binding of the two isomers to SWNTs was probed with NMR. The NMR spectrum (Figure 6) of the initial solution of **3** displays a 1:1 ratio of the two isomers, based on the integration of H^{α} peaks. After treatment with SWNTs, the NMR spectrum of the filtrate shows a 1:9 ratio of the *anti* and *syn* isomers, indicating that *anti*-**3** is bound to SWNTs in preference to *syn*-**3**. While *anti*-**3** and *syn*-**3** are similar chemically, they have very different shapes. The geometry-optimized structures of the two compounds are shown in Figure 7. The length of the molecule along the SWNT π—π interaction axis is 2.3 nm for the linear *anti*-**3** isomer (Figure 7A) and 1.5 nm for the bent *syn*-**3** isomer (Figure 7B), which suggests that *anti*-**3** has a larger surface area available to form π—π interactions with a neighboring SWNT. In both cases, the modification ratio of 3.2 molecules per (7,6) unit cell is very compact, as the length of a (7,6) unit cell is 4.8 nm, twice and three times the length of *anti*-**3** and *syn*-**3**, respectively. The side view of the isomers also shows a difference in the surface curvature between *anti*-**3** and *syn*-**3**. In the case of *anti*-**3**, the two fused-pyrene groups are slightly twisted in opposite directions (Figure 7C), which matches well with the surface curvature of (7,6) SWNTs. In the case of *syn*-**3**, the two fused-pyrene groups are curved in the same direction, distancing the π-system of *syn*-**3** from the SWNT surface (Figure 7D). Therefore we hypothesize that **3**-*anti* interacts more strongly with SWNTs compared to *syn*-**3** due to the larger π—π interaction area and favorable surface curvature of *anti*-**3**.

Photophysical Properties of 3—SWNTs. The photophysical properties of **3**—SWNTs were first studied by fluorescence experiments. Emission spectra were obtained by exciting the peak of the porphyrin Soret band. Before modification with SWNTs, strong NIR emission was observed for **3** at 830 nm in DMF. However upon

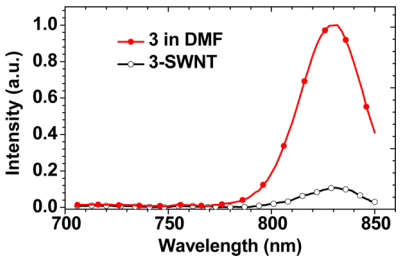

Figure 8. Emission spectra of 3 and 3−SWNT hybrids in DMF.

the formation of **3**−SWNTs, over 80% of the porphyrin emission was found to be quenched. This quenching may result from a variety of processes, including energy transfer from **3** to the bound SWNT or photoinduced charge separation.

To distinguish the excited-state kinetics that follow the photoexcitation of **3**, femtosecond transient absorption experiments were performed. Optical excitation of the porphyrin Q-band was achieved through an excitation pulse centered at 800 nm (Figure 9). Photobleaches corresponding to both the Soret (550 nm) and Q-bands (860 nm) of **3** appear immediately upon photoexcitation, indicating a depletion of the porphyrin's ground state. Interestingly, a photobleach at 660 nm that matches a feature in the absorption spectra of the unmodified SWNTs (Figure 2) also arises within the experiment's time resolution (100 fs). The concurrent growth of this feature along with photobleaches due to the porphyrin suggests that the electronic ground state of **3** partially extends onto the SWNT backbone. This observation is consistent with the large red-shift that occurs in the absorption spectrum of **3** upon binding to a SWNT, suggesting an extension of the π-system of **3**.

As the time delay between pump and probe is increased, the photobleaches corresponding to both the SWNT and Soret and Q-bands of **3** rapidly decay over the course of 1 ps. This result is qualitatively different from that observed in measurements of **3** dissolved in DMF (Figure S2). In these experiments, photoexcitation gives rise to Soret and Q-band photobleaches as well as a broad induced absorption band between these features. However, all of these features are long-lived compared to those seen following photoexcitation of **3**−SWNTs. Excitation of **3** in DMF leads to a photobleach and induced absorption features that decay exponentially with a rate constant of 1.8 ns and do not evolve spectrally with time. These observations, taken together with the fact that Zn-porphyrins generally have low intersystem crossing yields, suggest that the 1.8 ns time scale represents the sum of the rates for radiative and internal conversion pathways that directly return **3** to its ground state. Returning to the transient spectra of **3**−SWNT (Figure 9A), as the relaxation of the Soret and Q-band photobleaches occurs, a new induced absorption band

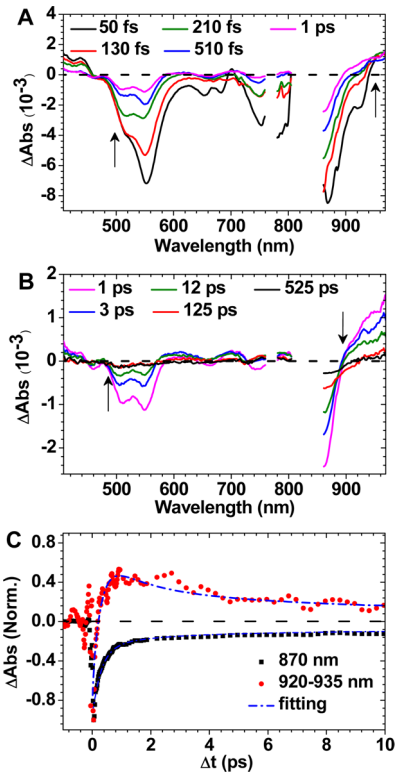

Figure 9. (A and B) Transient spectra measured for 3−SWNT hybrids in DMF following photoexcitation at 800 nm. (C) Temporal slices that correspond to the relaxation of the photobleach of the Q-band of 3 (black squares) and the induced absorption attributed to the cation of 3 (red circles). The dash dot blue lines correspond to biexponential fits with time constants of 260 fs and 6 ps.

appears at 900−970 nm, suggesting evolution from the initially populated S_1 state of **3** to a new excited state. This new absorption feature peaks at a time delay of 1 ps, decays over the course of a few tens of ps, and has largely vanished by 100 ps. Likewise, beyond 1 ps, the decay of the Q-band photobleach slows and tracks the relaxation of the induced absorption feature between 900 and 970 nm (Figure 9B). An isosbestic point at 890 nm can be observed between the Q-band bleach and the induced absorption band, indicating that the relaxation of this feature leads to a repopulation of the porphyrin's ground state. Both the growth and decay of the induced absorption band as well as the decay of the Q-band photobleach can be described by a biexponential function with time scales of 260 fs and 6 ps (Figure 9C).

The rapid photobleach loss and growth of a new absorption feature following the photoexcitation of **3** is unlikely to result from energy transfer from **3** to the SWNT backbone. Such a process would result in the return of **3** to its ground state, causing the photobleach of its Soret and Q-bands to fully recover as the new absorption feature appears. The fact that these bands show an additional slow decay that tracks the loss of the new absorption feature argues against this scenario. A more likely explanation for the observed spectral

evolution is that photoexcitation of **3** drives an electron transfer reaction between it and the bound SWNT. In this case, the appearance of new absorption features corresponding to both the cation of **3** and the SWNT anion are expected to appear. Furthermore, if these features overlap spectrally with the Soret and Q-bands of **3**, a decrease in the photobleach of these bands will be observed as the **3** cation and SWNT anion absorption features grow as the charge transfer reaction takes place. Once charge transfer has occurred, if charge recombination takes place that results in a nonradiative return of **3**–SWNT to its ground state, then both the photobleach of **3** and any cation/anion-induced absorption features will decay with the same time scale. Prior studies that have utilized pyrene-based linkers to tether electron-rich groups to SWNTs have observed photoinduced charge transfer between the tethered electron donor and SWNT,[44–47] but generally on longer time scales (a few ps to tens of ns) than the sub-ps decay observed here. However, the **3**–SWNT system described here differs from the materials investigated in these studies in that the doubly fused pyrene groups of **3** cause it to directly sit on the sidewall of the SWNT, leading to a smaller separation between the π-systems of **3** and the SWNT than in systems tethered to SWNTs *via* pyrene linkers.

To test if the spectral evolution we observe in the transient spectra can indeed be attributed to photoinduced electron transfer, we measured the cation absorption spectra of **3** by electrochemically oxidizing it in a cyclic voltammetry cell (Figure 10). The measured cation absorption spectrum shows a strong reduction in the intensity of both the Soret and Q-bands, but gains appreciable intensity to the red of both of these bands, notably near 600 nm and from 870 to 1000 nm. This latter region is the same spectral range over which the new absorption feature is observed in the transient spectra. Likewise, even though the intensities of the Soret and Q-bands are diminished in the cation absorption spectrum, the cation still shows an appreciable absorption in the range that these bands appear, lending support to the hypothesis that the sub-ps decay of the Soret and Q-bands arises from charge transfer. The rapidity with which charge transfer occurs in **3**–SWNT gives rise to the strong quenching observed in steady-state photoluminescence experiments (Figure 8).

Figure 11A plots transient spectra but now measured in the NIR spectral range after photoexcitation of the **3**–SWNT hybrid at 850 nm. A series of strong photobleach bands are found to arise within the instrument response, the most prominent of which appears at 1165 nm and matches a feature in the ground-state absorption spectrum of the **3**–SWNT hybrid that is attributable to the bound SWNT. Similar to what was observed for the Soret and Q-bands of **3**, after a delay of 1 ps, the decay of the SWNT photobleach tracks

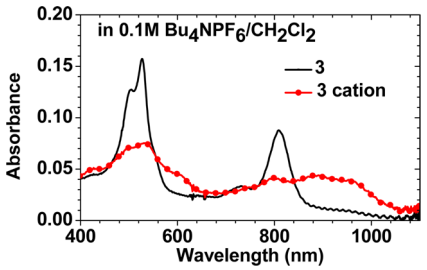

Figure 10. Absorption spectra of the porphyrin 3 cation measured through electrochemical oxidation.

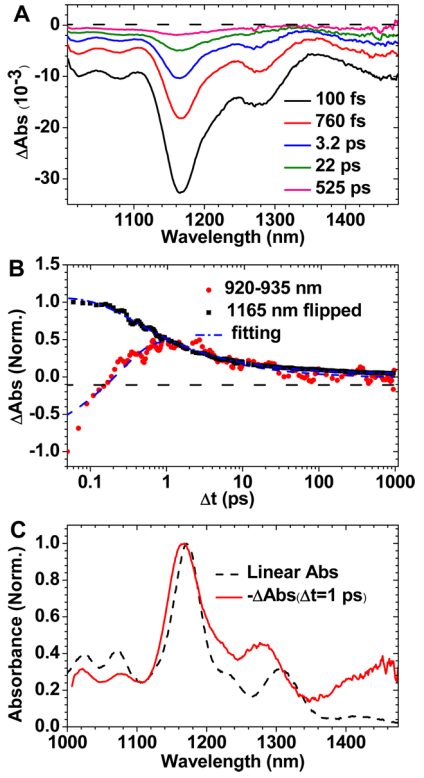

Figure 11. (A) Spectral slices showing the evolution of transient absorption spectra of 3–SWNT hybrids in the NIR spectral range following photoexcitation at 850 nm. (B) Temporal slices showing the relaxation of the photobleach of the SWNT (black squares) and 3 cation induced absorption (red circles). The sign of the SWNT photobleach has been inverted to enable better comparison with the 3 cation induced absorption profile. After 1 ps, these features show similar relaxation profiles. (C) Comparison of the absorption spectrum of 3–SWNT hybrids and the transient spectrum measured at a time delay of 1 ps.

the disappearance of the **3** cation (Figure 11B). This indicates that the electronic relaxation of the bound SWNT is linked to that of the porphyrin, as would be expected for the recombination of photogenerated charge carriers. At long time delays (~1 ns), the SWNT photobleach is found to relax to a 3% offset, indicating that a small amount of charge carriers persist in the system following photoexcitation.

Given that we observe induced absorption features that correspond to the cation of **3** following photoexcitation, we also expect to observe the appearance

of induced absorption features that are characteristic of SWNT anions. Prior transient absorptions of similar SWNT hybrid systems that undergo photoinduced charge transfer have attributed the appearance of induced absorption features between 1200 and 1600 nm to SWNT anions.[45] However, for the system studied here, no net induced absorption signal is observed in this spectral range. Rather, a comparison of the absorption spectrum of **3**−SWNT and the transient spectrum obtained at a 1 ps time delay where charge transfer is expected to be largely complete shows that the transient spectrum is not solely composed of a photobleach of ground-state absorption features. This may in part arise from contributions to the spectrum from weak SWNT anion induced absorption bands as well as a shift in the location of the van Hove singularities as a result of SWNT anion formation, as was observed in a tetrathiafulvalene-sensitized SWNT system.[43]

CONCLUSIONS

A systematic study of the binding between π-systems of fused pyrenylporphyrins and SWNTs has been reported. High solubility and unhindered π-system of fused pyrenylporphyrins allow efficient dispersion of SWNTs in common organic solvents, *e.g.*, toluene, CH_2Cl_2, and DMF. The binding of SWNTs to porphyrins has been found to be dependent on the length and shape of the porphyrin's π-system. While the nonfused porphyrin **1** shows only limited ability to solubilize SWNTs, the ability of porphyrins to bind to the SWNT surface increases across the series: monofused **2**, doubly fused *syn*-**3**, doubly fused *anti*-**3**. Very high selectivity in binding (>9:1) between different isomeric porphyrins with different π-system shapes has been observed. The linear π-system of the *anti*-**3** isomer fits well to a linear-shaped SWNT, resulting in improved binding to the surface of the SWNT compared to bent isomers with a similarly sized π-system. The formation of stable **3**−SWNT hybrids, characterized by UV−vis and SEM, allows further hierarchical modification by axial coordination of nitrogen-containing ligands to the porphyrin metal center to generate three-component nanohybrids. Transient absorption experiments indicate that while rapid photoinduced charge transfer occurs in **3**−SWNT hybrids ($1/k_{CT}$ = 260 fs), the majority of the photoinduced charges recombine over the course of a few picoseconds. This is the first example of strong electronic binding between π-extended porphyrins and SWNTs. Future modification of the nanohybrids through the addition of coordination ligands that move the positive charge further from the SWNT may be able to suppress the rapid charge recombination observed in the hybrids studied here, leading to a system suitable for applications in solar energy conversion.

SYNTHESIS AND EXPERIMENTAL METHODS

SWNTs used in our experiments were purification-grade HipCO SWNTs purchased from Unidym and CoMoCAT (7,6) SWNTs purchased from Sigma Aldrich; materials were used as purchased without any further purification. PTFE membranes with a pore size of 0.4 μm were purchased from Millipore. Ultrasonication (sonicator 3000, Misonix) was implemented by immersing an ultrasonic probe (standard 12.7 mm diameter tip) into 5−7 mL of the SWNT suspension. During sonication, the solution was immersed in an ice−water bath to prevent heating. Ultracentrifugation was performed using a Beckman XL-90. Absorption measurements were carried out using a Cary 14 UV−visible spectrometer, while steady-state emission measurements were performed using a Photon Technology International QuantaMaster model C-60 fluorimeter. TEM was performed on a JEOL JEM-2100 microscope at an operating voltage of 200 kV, equipped with a Gatan Orius CCD camera, and samples were prepared by drop casting SWNT suspensions onto 300 mesh Formvar-coated copper grids (Ted Pella, Inc.). ^{1}H NMR spectra were recorded on a Varian 400-MR spectrometer, and chemical shifts were reported in ppm relative to the residual nondeuterated solvent $CHCl_3$ (δ 7.26 ppm).

Ultrafast transient absorption experiments were conducted with a Ti:Sapphire regenerative amplifier operating at a 1kHz repetition rate (Coherent Legend, 3.5 mJ, 35 fs). Excitation pulses centered at 800 nm were derived from the direct output of the amplifier, while pulses centered at 850 nm were produced by pumping a visible OPA (Spectra Physics OPA-800C) with ~10% of the amplifier output. White light supercontinuum probe pulses were created by focusing a small amount of the amplifier output into either a 1 mm thick CaF_2 plate or a c-cut sapphire plate. CaF_2 was found to give a stable continuum from 320 to 1080 nm while sapphire yielded a continuum that extended further into the near-IR (450−1400 nm). To prevent photodamage, the CaF_2 plate was rotated slowly during data collection. Following its generation, the white light continuum was collimated and focused into the sample using a pair of off-axis aluminum parabolic mirrors. The pump was focused to a point after the sample with a CaF_2 lens to give a spot size of 300 μm (fwhm) at the sample. After passing through the sample, the probe was dispersed by a spectrograph (Oriel MS1271) onto a 256-element photodiode array. A Si diode array was used to measure spectra from 400 to 970 nm, while a thermoelectrically cooled InGaAs array (Hamamatsu G9213-256S) recorded transient spectra in the range 1000−1450 nm.

Samples for transient absorption experiments consisted of a solution of **3**−SWNT in DMF held in a 1 mm quartz cuvette. Samples were slowly translated perpendicular to the path of the pump and probe by a linear stage to prevent sample photodamage. The cross correlation of the pump and probe in a sample cuvette filled with neat DMF had an average fwhm of 100 fs across the probe spectrum. Transient spectra were recorded for a number of different pump energies between 60 and 900 nJ. Over this range, spectra were found to scale linearly with the pump fluence, suggesting that contributions to the spectra from bimolecular annihilation processes are minimal. For experiments that probe the NIR spectral range (Figure 11A), the sample concentration was adjusted such that the peak optical density of the Q-band of **3** was 0.3. A pump energy of 60 nJ was used, and the polarization between the pump and the probe was set to the magic angle. Due to the large scattering background in the visible region that arises from SWNTs, the sample concentration was lowered by 3× to record the spectra in Figure 9, and the pump energy was raised to 550 nJ. For this data set, the pump and probe were oriented perpendicular to one another. This allowed the suppression of scattered pump light by passing the probe through a polarizer after the sample.

Conflict of Interest: The authors declare no competing financial interest.

Acknowledgment. The authors thank the National Science Foundation for support of this research through the NSF-SOLAR program. S.T.R. would also like to acknowledge the National Science Foundation for support through an ACC-F fellowship (CHE-0937015). P.D.A. acknowledges the National Science Foundation for a Graduate Research Fellowship. The femtosecond transient absorption and TEM measurements were carried out with support from the Department of Energy's Energy Frontier Research Center program (Center for Energy Nanoscience, award DE-SC0001013).

Supporting Information Available: Photophysical characterization of porphyrin **3** in solution. This material is available free of charge *via* the Internet at http://pubs.acs.org.

REFERENCES AND NOTES

1. Iijima, S.; Ichihashi, T. Single-Shell Carbon Nanotubes of 1-nm Diameter. *Nature* **1993**, *364*, 737–737.
2. Kataura, H.; Kumazawa, Y.; Maniwa, Y.; Umezu, I.; Suzuki, S.; Ohtsuka, Y.; Achiba, Y. Optical Properties of Single-Wall Carbon Nanotubes. *Synth. Met.* **1999**, *103*, 2555–2558.
3. Bachilo, S. M.; Strano, M. S.; Kittrell, C.; Hauge, R. H.; Smalley, R. E.; Weisman, R. B. Structure-Assigned Optical Spectra of Single-Walled Carbon Nanotubes. *Science* **2002**, *298*, 2361–2366.
4. Dresselhaus, M. S.; Dresselhaus, G.; Saito, R.; Jorio, A. Raman Spectroscopy of Carbon Nanotubes. *Phys. Rep.* **2005**, *409*, 47–99.
5. Treacy, M. M. J.; Ebbesen, T. W.; Gibson, J. M. Exceptionally High Young's Modulus Observed for Individual Carbon Nanotubes. *Nature* **1996**, *381*, 678–680.
6. Wong, E. W.; Sheehan, P. E.; Lieber, C. M. Nanobeam Mechanics: Elasticity, Strength, and Toughness of Nanorods and Nanotubes. *Science* **1997**, *277*, 1971–1975.
7. Yu, M. F.; Files, B. S.; Arepalli, S.; Ruoff, R. S. Tensile Loading of Ropes of Single Wall Carbon Nanotubes and Their Mechanical Properties. *Phys. Rev. Lett.* **2000**, *84*, 5552–5555.
8. Wildoer, J. W. G.; Venema, L. C.; Rinzler, A. G.; Smalley, R. E.; Dekker, C. Electronic Structure of Atomically Resolved Carbon Nanotubes. *Nature* **1998**, *391*, 59–62.
9. Javey, A.; Guo, J.; Wang, Q.; Lundstrom, M.; Dai, H. J. Ballistic Carbon Nanotube Field-Effect Transistors. *Nature* **2003**, *424*, 654–657.
10. Schnorr, J. M.; Swager, T. M. Emerging Applications of Carbon Nanotubes. *Chem. Mater.* **2011**, *23*, 646–657.
11. Heller, D. A.; Jin, H.; Martinez, B. M.; Patel, D.; Miller, B. M.; Yeung, T. K.; Jena, P. V.; Hobartner, C.; Ha, T.; Silverman, S. K.; *et al*. Multimodal Optical Sensing and Analyte Specificity Using Single-Walled Carbon Nanotubes. *Nat. Nanotechnol.* **2009**, *4*, 114–120.
12. Kauffman, D. R.; Star, A. Electronically Monitoring Biological Interactions with Carbon Nanotube Field-Effect Transistors. *Chem. Soc. Rev.* **2008**, *37*, 1197–1206.
13. Rowell, M. W.; Topinka, M. A.; McGehee, M. D.; Prall, H. J.; Dennler, G.; Sariciftci, N. S.; Hu, L. B.; Gruner, G. Organic Solar Cells with Carbon Nanotube Network Electrodes. *Appl. Phys. Lett.* **2006**, 88.
14. Kostarelos, K.; Bianco, A.; Prato, M. Promises, Facts and Challenges for Carbon Nanotubes in Imaging and Therapeutics. *Nat. Nanotechnol.* **2009**, *4*, 627–633.
15. Cataldo, S.; Salice, P.; Menna, E.; Pignataro, B. Carbon Nanotubes and Organic Solar Cells. *Energy Environ. Sci.* **2012**, *5*, 5919–5940.
16. Baughman, R. H.; Zakhidov, A. A.; de Heer, W. A. Carbon Nanotubes - The Route toward Applications. *Science* **2002**, *297*, 787–792.
17. Tasis, D.; Tagmatarchis, N.; Bianco, A.; Prato, M. Chemistry of Carbon Nanotubes. *Chem. Rev.* **2006**, *106*, 1105–1136.
18. Zhao, Y. L.; Stoddart, J. F. Noncovalent Functionalization of Single-Walled Carbon Nanotubes. *Acc. Chem. Res.* **2009**, *42*, 1161–1171.
19. Zhang, Z. X.; Che, Y. K.; Smaldone, R. A.; Xu, M. A.; Bunes, B. R.; Moore, J. S.; Zang, L. Reversible Dispersion and Release of Carbon Nanotubes Using Foldable Oligomers. *J. Am. Chem. Soc.* **2010**, *132*, 14113–14117.
20. Lemasson, F. A.; Strunk, T.; Gerstel, P.; Hennrich, F.; Lebedkin, S.; Barner-Kowollik, C.; Wenzel, W.; Kappes, M. M.; Mayor, M. Selective Dispersion of Single-Walled Carbon Nanotubes with Specific Chiral Indices by Poly(*N*-decyl-2,7-carbazole). *J. Am. Chem. Soc.* **2011**, *133*, 652–655.
21. Guldi, D. M.; Rahman, G. M. A.; Zerbetto, F.; Prato, M. Carbon Nanotubes in Electron Donor-Acceptor Nanocomposites. *Acc. Chem. Res.* **2005**, *38*, 871–878.
22. Romero-Nieto, C.; Garcia, R.; Herranz, M. A.; Ehli, C.; Ruppert, M.; Hirsch, A.; Guldi, D. M.; Martin, N. Tetrathiafulvalene-Based Nanotweezers-Noncovalent Binding of Carbon Nanotubes in Aqueous Media with Charge Transfer Implications. *J. Am. Chem. Soc.* **2012**, *134*, 9183–9192.
23. Arnold, M. S.; Zimmerman, J. D.; Renshaw, C. K.; Xu, X.; Lunt, R. R.; Austin, C. M.; Forrest, S. R. Broad Spectral Response Using Carbon Nanotube/Organic Semiconductor/C-60 Photodetectors. *Nano Lett.* **2009**, *9*, 3354–3358.
24. Fuhrer, M. S.; Durkop, T.; Getty, S. A.; Cobas, E. Extraordinary Mobility in Semiconducting Carbon Nanotubes. *Nano Lett.* **2004**, *4*, 35–39.
25. D'Souza, F.; Sandanayaka, A. S. D.; Ito, O. SWNT-Based Supramolecular Nanoarchitectures with Photosensitizing Donor and Acceptor Molecules. *J. Phys. Chem. Lett.* **2010**, *1*, 2586–2593.
26. Bartelmess, J.; Ballesteros, B.; de la Torre, G.; Kiessling, D.; Campidelli, S.; Prato, M.; Torres, T.; Guldi, D. M. Phthalocyanine-Pyrene Conjugates: A Powerful Approach toward Carbon Nanotube Solar Cells. *J. Am. Chem. Soc.* **2010**, *132*, 16202–16211.
27. Murakami, H.; Nomura, T.; Nakashima, N. Noncovalent Porphyrin-Functionalized Single-Walled Carbon Nanotubes in Solution and the Formation of Porphyrin–Nanotube Nanocomposites. *Chem. Phys. Lett.* **2003**, *378*, 481–485.
28. Li, H. P.; Zhou, B.; Lin, Y.; Gu, L. R.; Wang, W.; Fernando, K. A. S.; Kumar, S.; Allard, L. F.; Sun, Y. P. Selective Interactions of Porphyrins with Semiconducting Single-Walled Carbon Nanotubes. *J. Am. Chem. Soc.* **2004**, *126*, 1014–1015.
29. Cheng, F. Y.; Zhang, S.; Adronov, A.; Echegoyen, L.; Diederich, F. Triply Fused Zn-II-Porphyrin Oligomers: Synthesis, Properties, and Supramolecular Interactions with Single-Walled Carbon Nanotubes (SWNTs). *Chem.—Eur. J.* **2006**, *12*, 6062–6070.
30. Cheng, F. Y.; Zhu, J. S.; Adronov, A. Supramolecular Functionalization of Single-Walled Carbon Nanotubes with Triply Fused Porphyrin Dimers: A Study of Structure-Property Relationships. *Chem. Mater.* **2011**, *23*, 3188–3194.
31. Cheng, F. Y.; Adronov, A. Noncovalent Functionalization and Solubilization of Carbon Nanotubes by Using A Conjugated Zn-Porphyrin Polymer. *Chem.—Eur. J.* **2006**, *12*, 5053–5059.
32. Lewtak, J. P.; Gryko, D. T. Synthesis of π-Extended Porphyrins *via* Intramolecular Oxidative Coupling. *Chem. Commun.* **2012**, *48*, 10069–10086.
33. Pereira, A. M. V. M.; Richeter, S.; Jeandon, C.; Gisselbrecht, J. P.; Wytko, J.; Ruppert, R. Synthesis of Extended Porphyrins by Connection of meso-Aryl Groups with β-Pyrrolic Positions. *J. Porphyrins Phthalocyanines* **2012**, *16*, 464–478.
34. Kurotobi, K.; Kim, K. S.; Noh, S. B.; Kim, D.; Osuka, A. A Quadruply Azulene-Fused Porphyrin with Intense Near-IR Absorption and a Large Two-Photon Absorption Cross Section. *Angew. Chem., Int. Ed.* **2006**, *45*, 3944–3947.
35. Tanaka, M.; Hayashi, S.; Eu, S.; Umeyama, T.; Matano, Y.; Imahori, H. Novel Unsymmetrically π-Elongated Porphyrin for Dye-Sensitized TiO_2 Cells. *Chem. Commun.* **2007**, 2069–2071.
36. Jiao, C. J.; Huang, K. W.; Guan, Z. P.; Xu, Q. H.; Wu, J. S. N-Annulated Perylene Fused Porphyrins with Enhanced Near-IR Absorption and Emission. *Org. Lett.* **2010**, *12*, 4046–4049.
37. Davis, N. K. S.; Thompson, A. L.; Anderson, H. L. A Porphyrin Fused to Four Anthracenes. *J. Am. Chem. Soc.* **2011**, *133*, 30–31.

38. Diev, V. V.; Hanson, K.; Zimmerman, J. D.; Forrest, S. R.; Thompson, M. E. Fused Pyrene-Diporphyrins: Shifting Near-Infrared Absorption to 1.5 μm and Beyond. *Angew. Chem., Int. Ed.* **2010**, *49*, 5523–5526.
39. Diev, V. V.; Schlenker, C. W.; Hanson, K.; Zhong, Q. W.; Zimmerman, J. D.; Forrest, S. R.; Thompson, M. E. Porphyrins Fused with Unactivated Polycyclic Aromatic Hydrocarbons. *J. Org. Chem.* **2012**, *77*, 143–159.
40. Tomonari, Y.; Murakami, H.; Nakashima, N. Solubilization of Single-Walled Carbon Nanotubes by Using Polycyclic Aromatic Ammonium Amphiphiles in Water - Strategy for the Design of High-Performance Solubilizers. *Chem. —Eur. J.* **2006**, *12*, 4027–4034.
41. Sprafke, J. K.; Stranks, S. D.; Warner, J. H.; Nicholas, R. J.; Anderson, H. L. Noncovalent Binding of Carbon Nanotubes by Porphyrin Oligomers. *Angew. Chem., Int. Ed.* **2011**, *50*, 2313—2316.
42. Dai, H. J.; Chen, R. J.; Zhang, Y. G.; Wang, D. W. Noncovalent Sidewall Functionalization of Single-Walled Carbon Nanotubes for Protein Immobilization. *J. Am. Chem. Soc.* **2001**, *123*, 3838–3839.
43. Ehli, C.; Rahman, G. M. A.; Jux, N.; Balbinot, D.; Guldi, D. M.; Paolucci, F.; Marcaccio, M.; Paolucci, D.; Melle-Franco, M.; Zerbetto, F.; *et al.* Interactions in Single Wall Carbon Nanotubes/Pyrene/Porphyrin Nanohybrids. *J. Am. Chem. Soc.* **2006**, *128*, 11222–11231.
44. Harranz, M. Á.; Ehil, C.; Campidelli, S.; Gutiérrez, M.; Hug, G. L.; Ohkubo, K.; Fukuzumi, S.; Prato, M.; Martín, N.; Guldi, D. M. Spectroscopic Characterization of Photolytically Generated Radical Ion Pairs in Single-Wall Carbon Nanotubes Bearing Surface-Immolilized Tetrathiafulvalenes. *J. Am. Chem. Soc.* **2008**, *130*, 66–73.
45. Sandanayaka, A. S. D.; Chitta, R.; Subbaiyan, N. K.; D'Souza, L.; Ito, O.; D'Souza, F. Photoinduced Charge Separation in Ion-Paired Porphyrin-Single-Wall Carbon Nanotube Donor-Acceptor Hybrids. *J. Phys. Chem. C* **2009**, *113*, 13425–13432.
46. Maligaspe, E.; Sandanayaka, A. S. D.; Hasobe, T.; Ito, O.; D'Souza, F. Sensitive Efficiency of Photoinduced Electron Transfer to Band Gaps of Semiconductive Single-Walled Carbon Nanotubes with Supramolecularly Attached Zinc Porphyrin Bearing Pyrene Glues. *J. Am. Chem. Soc.* **2010**, *132*, 8158–8164.
47. Bartelmess, J.; Ballesteros, B.; Torre, G. d. l.; Kiessling, D.; Campidelli, S.; Prato, M.; Torres, T.; Guldi, D. M. Phthalocyanine-Pyrene Conjugates: A Powerful Approach toward Carbon Nanotube Solar Cells. *J. Am. Chem. Soc.* **2010**, *132*, 16202–16211.